Mon. Not. R. Astron. Soc. **000**, 1–16 () Printed 26 March 2009 (MN LATEX style file v2.2)

Oscillations of rapidly rotating stratified neutron stars

A. Passamonti⋆ , B. Haskell, N. Andersson, D.I. Jones and I. Hawke

School of Mathematics, University of Southampton, Southampton SO17 1BJ, UK

26 March 2009

ABSTRACT

We use time-evolutions of the linear perturbation equations to study the oscillations of rapidly rotating neutrons stars. Our models account for the buoyancy due to composition gradients and we study, for the first time, the nature of the resultant g-modes in a fast spinning star. We provide detailed comparisons of non-stratified and stratified models. This leads to an improved understanding of the relationship between the inertial modes of a non-stratified star and the g-modes of a stratified system. In particular, we demonstrate that each g-mode becomes rotation-dominated, i.e. approaches a particular inertial mode, as the rotation rate of the star is increased. We also discuss issues relating to the gravitational-wave driven instability of the various classes of oscillation modes.

Key words: methods: numerical – stars: neutron – stars: oscillation – star:rotation.

1 INTRODUCTION

The oscillations of rotating neutron stars are of great interest in astrophysics. Recent efforts to understand the various pulsation modes of compact stars have to a large extent been motivated by gravitational-wave astronomy (Andersson & Kokkotas 1996, 1998). Different modes of oscillation depend on different pieces of internal physics and one may hope to use observations to probe, for example, the composition of the high-density region (Ferrari & Gualtieri 2008; Benhar et al. 2007). Work in this area, which has a long history (for a review see e.g., Kokkotas & Schmidt 1999), gained further momentum recently with the relatively successful matching between observed quasiperiodic oscillations in the tails of magnetar flares and calculated torsional oscillations of the neutron star crust (Duncan 1998; Piro 2005; Watts & Strohmayer 2007; Samuelsson & Andersson 2007). The excitement following these, the first ever, observations of likely neutron star vibrations is significant. It is clear that our models need to be improved significantly if we expect to carry out a quantitative astero-seismology programme for neutron stars, but the prospects for improvements look good. After all, we already have a reasonable understanding of the dynamics of the crust region (see Carter & Samuelsson 2006; Samuelsson & Andersson 2007) as well as the superfluid components in the core of the star (Andersson & Comer 2007).

The present work is motivated by the need to consider more realistic models of rapidly rotating stars. Our emphasis will be on the role of the internal stratification associated with composition variations. This leads to the presence of the so-called g-modes (Reisenegger & Goldreich 1992), and we want to investigate how these modes are affected by fast rotation (the analogous problem for thermal ocean g-modes of rapidly rotating neutron stars has already been considered, see Bildsten, Ushomirsky & Cutler (1996)). In order to determine the rotational effects on the oscillation spectrum we study linear perturbations of axisymmetric stellar configurations, where the Coriolis force and the centrifugal flattening of the star are included in the background. In this way, we go beyond the so-called slow rotation approximation, where the rotation itself is treated perturbatively and the mode-frequencies of non-rotating models are determined by a perturbation expansion with respect to the angular velocity of the star Ω. We are particularly interested in the relationship between the g-modes of a stratified stellar model and the inertial modes (Lockitch & Friedman 1999), for which the Coriolis force is the main restoring agent. The inertial modes are important since they may be driven unstable by the emission of gravitational waves. The strongest instability is associated with the so-called r-modes (Andersson & Kokkotas 2001; Andersson 2003). A key issue

⋆ E-mail:a.passamonti@soton.ac.uk

concerns the amplitude at which an unstable mode saturates. Detailed work has shown that an unstable r-mode saturates due to nonlinear couplings to other inertial modes (Arras et al. 2003). However, the mode saturation has only been considered for slowly rotating, non-stratified models and it is important to ask to what extent these results will change if the models are made more realistic. In stratified neutron stars, the g-modes tend to become rotationally dominated beyond a certain rotation rate (see e.g., Yoshida & Lee 2000; Dintrans & Rieutord 2000) and may then be called inertia-gravity modes (Unno et al. 1989). Effects due to the stratification are thus weakened, which indicates that the r-mode saturation estimates may still be reliable, at least for the fastest spinning systems.

Improving and extending a numerical code that has been used to study non-stratified stars (Jones, Andersson & Stergioulas 2002), we approach the problem via time-evolutions of the equations that govern the linear perturbations of a, potentially rapidly, rotating Newtonian star. This strategy has the advantage that one does not have to deal with the many rotationally coupled multipoles, that tend to make a slow-rotation calculation less tractable. On the other hand, a numerical evolution is not expected to have the precision of a frequency domain calculation. Neither should one expect it to yield the complete spectrum of modes. After all, the simulation results depend on the chosen initial data. In absence of a clear idea of the nature of the various modes one does not know how to excite specific oscillations. One way around this problem is to follow the "recycling" strategy developed by Stergioulas, Apostolatos & Font (2004) and Dimmelmeier, Stergioulas & Font (2006). Another, more pragmatic, approach is to simply study the modes that are excited by "generic" initial data. This is the attitude that we adopt here.

2 ROTATING STELLAR MODELS

We want to investigate the effect that composition variations have on the various oscillation modes of a rapidly rotating neutron star. To do this, we consider an equilibrium configuration representing a rapidly and uniformly rotating star containing three particle species. We assume that matter is composed of degenerate neutrons n, protons p and electrons e. For simplicity, we further assume that neutrons and protons are not superfluid. In essence, our model represents the conditions in the outer core of a very young neutron star that has not yet cooled below the temperature at which the baryons form superfluid condensates (in practice with a core temperature significantly above 10^9 K). We also do not consider the various exotic phases of matter that may be present in the deep core of a realistic neutron star model, e.g. hyperons or deconfined quarks (see Lattimer & Prakash 2004, 2007). Accounting for the presence of such phases would not be too difficult, but at this stage our focus is on understanding the basic role of composition variations. We are already extending this work to account for the presence of superfluid components and expect to report on results in this direction soon.

The matter composition is represented by the three number densities $n_{\rm x}$, where x is either n, p or e. Charge neutrality is provided by the Coulomb interaction, that efficiently lock together protons and electrons (e.g., Villain, Bonazzola & Haensel 2005). Thus we have $n_{\rm p} = n_{\rm e}$ and $\mathbf{v}_{\rm p} = \mathbf{v}_{\rm e}$, where $\mathbf{v}_{\rm x}$ denotes the velocity of each fluid component. In this model, the pressure P is a function of two variables, e.g. the neutron and proton number densities or alternatively the total baryon number density $n_{\rm b} = n_{\rm n} + n_{\rm p}$ and the proton fraction $x_{\rm p} = n_{\rm p}/n_{\rm b}$. In the unperturbed stellar model, it is assumed that the weak interaction processes:

$$n \longrightarrow p + e + \bar{\nu}_{\rm e}\,, \qquad\qquad p + e \longrightarrow n + \nu_{\rm e}\,, \tag{1}$$

lead to β-equilibrium. The proton fraction is then only a function of the baryon number density (or equivalently the baryon mass density $\rho = m\,(n_{\rm p} + n_{\rm n})$, where for simplicity the proton and neutron masses have been assumed equal). Then the stellar fluid can be described by a barotropic equation of state $P = P\,(\rho)$. In this paper, we consider a simple polytropic model

$$P = K\rho^{\Gamma_\beta}\,, \tag{2}$$

where K is constant and

$$\Gamma_\beta \equiv \frac{d\log P}{d\log\rho}\,, \tag{3}$$

is the adiabatic index.

Once the equation of state is provided, rotating stellar configurations can be determined by the Hachisu self-consistent field method (Hachisu 1986). For this purpose we use the numerical code described in Jones et al. (2002). This code generates axisymmetric equilibrium models by specifying the polytropic index and the ratio of the polar to equatorial axes R_p/R_{eq}. In Table 1 we give some details relating to the rotation rate, energies and masses of equilibrium configurations used in this paper.

3 THE PERTURBATION PROBLEM

In a perturbed configuration, an oscillating fluid element may not have time to reach β-equilibrium with the neighbouring matter. In fact, for typical stellar oscillation frequencies the time scale of the weak interaction processes is much too long for

Table 1. This table displays the main quantities of our rotating equilibrium configurations. The stellar models are described by a polytropic equation of state with adiabatic index $\Gamma_\beta = 2$. In the first and second columns we show, respectively, the ratio of polar to equatorial axes and the angular velocity of the star. In the third column, the rotation rate is compared to the Kepler velocity Ω_K that represents the mass shedding limit. The ratio between the rotational kinetic energy and gravitational potential energy $T/|W|$ and the stellar mass are given in the fourth and fifth columns, respectively. All quantities are given in dimensionless units, where G is the gravitational constant, ρ_c represents the central mass density and R_{eq} is the equatorial radius.

R_p/R_{eq}	$\Omega/\sqrt{G\rho_c}$	Ω/Ω_K	$T/\|W\| \times 10^2$	$M/(\rho_c R_{eq}^3)$
1.000	0.000	0.000	0.000	1.273
0.996	0.084	0.116	0.096	1.270
0.992	0.119	0.164	0.192	1.261
0.983	0.167	0.230	0.385	1.248
0.950	0.287	0.396	1.170	1.197
0.933	0.331	0.456	1.570	1.171
0.900	0.403	0.556	2.380	1.118
0.850	0.488	0.673	3.640	1.038
0.800	0.556	0.767	4.930	0.956
0.750	0.612	0.844	6.250	0.869
0.700	0.658	0.907	7.570	0.779
0.650	0.693	0.956	8.820	0.684
0.600	0.717	0.989	9.860	0.579

the matter to equilibrate within one oscillation period (e.g., Reisenegger & Goldreich 1992). In the limit of slow reactions one can thus accurately assume that the composition of a perturbed fluid element is frozen. This condition can be imposed by letting the Lagrangian variation of the proton fraction vanish, i.e.,

$$\Delta x_{\rm p} = \delta x_{\rm p} + \xi \cdot \nabla x_{\rm p} = 0\,, \tag{4}$$

where ξ denotes the Lagrangian displacement of a fluid element.

The perturbed fluid is no longer described by the one-parameter equation of state that determined the background model. The perturbed pressure now depends on both the proton fraction and the baryon density,

$$\delta P = \delta P\left(\rho, x_{\rm p}\right)\,. \tag{5}$$

Given equation (4), the Lagrangian perturbation of pressure is given by

$$\Delta P = \Gamma_{\rm f} \frac{P}{\rho}\,\Delta\rho\,, \tag{6}$$

where

$$\Gamma_{\rm f} \equiv \left.\frac{\partial \log P}{\partial \log \rho}\right|_{x_{\rm p}}\,, \tag{7}$$

is the adiabatic index for a frozen composition. Alternatively, equation (6) can be written in terms of Eulerian perturbations;

$$\frac{\delta\rho}{\rho} = \frac{1}{\Gamma_{\rm f}}\frac{\delta P}{P} - \xi\cdot\mathbf{A}\,. \tag{8}$$

The vector field $\mathbf{A}$ is defined as

$$\mathbf{A} \equiv \nabla \ln\rho - \frac{1}{\Gamma_{\rm f}}\nabla \ln P = \left(\frac{1}{\Gamma_\beta} - \frac{1}{\Gamma_{\rm f}}\right)\nabla \ln P\,. \tag{9}$$

Its magnitude is usually referred to as the Schwarzschild discriminant, with an overall sign depending upon whether $\mathbf{A}$ points outward (positive discriminant) or inward (negative discriminant). Note that the background relation (3) has been used in the last equality of equation (9).

For barotropic stellar oscillations a single equation of state describes both the background and the perturbed matter. The adiabatic indices Γ_β and $\Gamma_{\rm f}$ are then equal and the Schwarzshild discriminant vanishes, $\mathbf{A} = 0$. In this case, the stellar structure does not sustain buoyancy restored modes so the composition g-modes are absent from the spectrum (Reisenegger & Goldreich 1992). In the nonbarotropic case, $\mathbf{A} \neq 0$, the sign of the Schwarzschild discriminant determines the convective stability of the motion. Stable (unstable) g modes are present in stars with negative (positive) Schwarzschild discriminant (Tassoul 1978; Unno et al. 1989).

In our numerical evolutions, we do not use the Lagrangian displacement ξ as a dynamical variable. Instead we evolve the perturbed proton fraction $\delta x_{\rm p}$. The relevant dynamical equation follows if we rewrite equation (8) using equation (4);

$$\frac{\delta\rho}{\rho} = \frac{1}{\Gamma_{\rm f}}\frac{\delta P}{P} - \left(\frac{\Gamma_\beta}{\Gamma_{\rm f}} - 1\right)\frac{\delta\chi_{\rm p}}{\rho}\,, \tag{10}$$

where we have defined

$$\delta\chi_{\rm p} \equiv \delta x_{\rm p} / \left(\frac{dx_{\rm p}}{d\rho}\right) . \tag{11}$$

We have also assumed that $x_{\rm p} = x_{\rm p}(\rho)$.

The composition gradient can be directly related to the deviation of $\Gamma_{\rm f}$ from the background Γ_β. From equation (5) the pressure perturbation can be expressed as

$$\frac{\delta P}{P} = \Gamma_{\rm f}\frac{\delta\rho}{\rho} + \Gamma_{\rm p}\frac{\delta x_{\rm p}}{x_{\rm p}} , \tag{12}$$

where

$$\Gamma_{\rm p} \equiv \left.\frac{d\log P}{d\log x_{\rm p}}\right|_\rho . \tag{13}$$

Comparing equations (10) and (12) we obtain the following relation between the proton fraction and the adiabatic indices:

$$\Gamma_\beta - \Gamma_{\rm f} = \Gamma_{\rm p}\frac{d\log x_{\rm p}}{d\log\rho} . \tag{14}$$

It is now straightforward to extend the models considered by Jones et al. (2002) to account for composition variations. Non-axisymmetric perturbations of rapidly, and uniformly, rotating stratified neutron stars can be described by a system of five equations. This system is formed by the perturbed Euler, mass conservation and frozen composition equations. In the frame of the rotating background and in terms of the dynamical variables δP, $\delta\chi_{\rm p}$ and the flux $\mathbf{f} = \rho\,\mathbf{v}$, the equations can be written

$$\partial_t \mathbf{f} = -\nabla\delta P - 2\left(\mathbf{\Omega}\times\mathbf{f}\right) + \frac{\nabla\ln P}{\Gamma_{\rm f}}\delta P + \left(1-\frac{\Gamma_\beta}{\Gamma_{\rm f}}\right)\frac{\nabla P}{\rho}\delta\chi_{\rm p} , \tag{15}$$

$$\partial_t \delta P = -\Gamma_{\rm f}\frac{P}{\rho}\nabla\cdot\mathbf{f} + \frac{1}{\rho}\left(\frac{\Gamma_{\rm f}}{\Gamma_\beta}-1\right)\mathbf{f}\cdot\nabla P , \tag{16}$$

$$\partial_t \delta\chi_{\rm p} = -\frac{\mathbf{f}\cdot\nabla P}{\Gamma_\beta P} . \tag{17}$$

In writing down equation (15) we have made the Cowling approximation, i.e. neglected the forces due to the perturbed gravitational potential. Equation (17) describes the conservation of the proton fraction in a fluid element moving with the fluid. It is equivalent to the time derivative of equation (4). For $\Gamma_\beta = \Gamma_{\rm f}$, the system of equations (15)-(17) reduces to the barotropic perturbation equations considered in Jones et al. (2002). In that case, $\delta\chi_{\rm p}$ is a superfluous dynamical variable.

As is clear from the above equations, time evolution of the non-axisymmetric perturbation equations is a three-dimensional problem in space. However, by exploiting the axial symmetry of the stellar background and the fact that we only consider linear perturbations, all perturbed variables can be expanded in terms of a set of basis functions $(\cos m\phi\,, \sin m\phi)$, where m is the azimuthal harmonic index (Papaloizou & Pringle 1980). For instance, in the case of the pressure we have

$$\delta P(t,r,\theta,\phi) = \sum_{m=0}^{m=\infty}\left[\delta P_m^+(t,r,\theta)\cos m\phi + \delta P_m^-(t,r,\theta)\sin m\phi\right] , \tag{18}$$

The perturbation equations then decouple with respect to m and the problem becomes two-dimensional. For any m, the non-axisymmetric oscillations of a stratified neutron star requires the solution of a system of ten partial differential equations for the ten variables $\left(\delta P^\pm, \mathbf{f}^\pm, \delta\chi_{\rm p}^\pm\right)$.

4 BOUNDARY CONDITIONS

The evolution equations need to be complemented by boundary conditions. At the stellar surface we require that the Lagrangian perturbation of the pressure vanishes, i.e.,

$$\Delta P = \delta P + \xi\cdot\nabla P = 0 . \tag{19}$$

From the Euler equation for the stationary background

$$\nabla P = -\rho\mathbf{\Omega}\times(\mathbf{\Omega}\times\mathbf{r}) - \rho\nabla\Phi , \tag{20}$$

the condition (19) reduces to

$$\Delta P = \delta P - \rho\xi\cdot(\mathbf{\Omega}\times\mathbf{\Omega}\times\mathbf{r} + \nabla\Phi) = 0 . \tag{21}$$

In a polytropic star, the mass density vanishes on the stellar surface. Therefore, if the Lagrangian displacement ξ assumes finite values at the surface, according to equation (21) the pressure perturbation δP behaves as ρ near the surface. In order to avoid divergent solutions in the numerical simulations, we impose a zero surface condition for the mass flux perturbation

$$\mathbf{f} = \rho\mathbf{v} = 0 . \tag{22}$$

We consider initial conditions where the Lagrangian displacement is finite on the stellar surface. Therefore, equation (22) implies that along the numerical evolution also the quantity $\rho\xi$ remains zero on the surface. As a result, from equation (21) the Eulerian pressure perturbation satisfies a zero surface condition

$$\delta P = 0\,. \tag{23}$$

This condition ensures that the perturbed quantities remain regular at the surface. It is also straightforward to implement in the code.

We focus on the non-axisymmetric oscillations for $m \geqslant 2$. At the origin, $r = 0$, the regular behaviour of equations (15)-(17) is then guaranteed by the conditions:

$$\delta P = \delta\chi_{\rm p} = \mathbf{f} = 0\,. \tag{24}$$

5 OSCILLATION MODES OF ROTATING STARS

Before we discuss the results of our evolutions, it is useful to digress on the expected nature of the pulsation modes of a spinning star.

Perturbations of spherical (non-spinning) stars can be decomposed in two separate classes identified by their behaviour under the parity transformation. Polar perturbations, which are expressed in terms of the scalar spherical harmonics Y_{lm} and their gradients ∇Y_{lm}, transform as $(-1)^l$ under parity inversion. Meanwhile, axial perturbations, which behave as $r \times \nabla Y_{lm}$, change sign as $(-1)^{l+1}$ under parity. In a spherical star, the different multipoles do not couple. An oscillation mode can be identified by the harmonic indices l and m (together with some statement about the radial eigenfunction).

For rotating stars, the problem is more complicated. First of all, rotation removes the degeneracy in m generating a richer spectrum than in a non-rotating star. Secondly, the identification of a mode with a single l is well defined only for non-rotating models. Nevertheless, each individual mode can be tracked by increasing the rotation rate step by step. It is also important to note that, even though the spectral properties of an oscillation mode change continuously along a sequence of rotating models, its overall parity is conserved.

In this paper we discuss the three main classes of oscillation modes. They are classified according to the dominant restoring force that acts on the perturbed fluid elements (Cowling 1941). For polar modes the high frequency part of the spectrum, roughly above 1 kHz, is occupied by the fundamental f-mode and the acoustic p-modes. In stars where composition or thermal gradients are present, low-frequency g-modes are also present. These are restored by gravity through the buoyancy force. These various modes are non-trivial already in a non-rotating star. A polar mode labeled by the harmonic index l in a non-rotating configuration is split by rotation into $2l + 1$ distinct modes (identified by the value of m).

In contrast, there are no non-trivial axial modes in a non-rotating fluid star. The axial modes form a zero frequency subspace that describe stationary convective currents (Lockitch & Friedman 1999). In a rotating configuration, these modes become non-trivial thanks to the Coriolis force. Collectively, they are referred to as inertial modes. A general mode in this rotation-dominated class can have a mixture of axial and polar components. However, since each mode has a distinct parity one can distinguish two separate classes of inertial modes. Following Lockitch & Friedman (1999) we refer to these sets as polar- and axial-led. In the family of axial-led inertial modes, you find the so-called r-modes. They are particularly simple in that they are purely axial in the slow-rotation limit. For barotropic stars only the $l = m$ r-modes exist, while in non-barotropic stars $l \neq m$ r-modes also appear. An interesting question concerns the fate of these r-modes in the barotropic limit. Some aspects of this question were resolved by Lockitch & Friedman (1999), but interesting questions remain. Consider, for example, a weakly stratified star. In a fast spinning configuration the buoyancy should be dominated by the Coriolis force and the low frequency modes should essentially have an inertial nature. For lower rotation rates there should be a transition to a buoyancy dominated regime, where the g-modes become distinct. Of course, the relative strength of the Coriolis force and the buoyancy will vary throughout a star. As we will discuss in Section 7.3 one would expect to find distinct regions where buoyancy dominates the Coriolis force, and other regions where it is less important (Dintrans & Rieutord 2000). It is then important to understand these two regions better. One would certainly want to know if it is possible to track individual modes from one regime to the other. Ideally, this would shed some light on the relationship between the inertial modes of a barotropic model and the g-modes of a non-barotropic system.

Let us finally make a connection between the various classes of modes and our evolution problem. In the evolutions, we do not distinguish between axial and polar perturbations. Instead, we use the fact that perturbations of an axisymmetric background can be decomposed into two parity classes that satisfy different conditions in the equatorial plane. For the first class, which we will refer to as type I parity, $\delta P^+, \delta\chi_{\rm p}^+, f_r^+, f_\phi^+$ are all even under reflection with respect to the equatorial plane, while f_θ^- is odd. The $l = m$ fundamental modes and the polar-led inertial modes belong to this class. Conversely, for the second class, that we will refer to as type II parity, $\delta P^-, \delta\chi_{\rm p}^-, f_r^-, f_\phi^-$ are odd and f_θ^+ is even. Typical modes of a rotating star that belong to this parity class are the $l + 1 = m$ fundamental modes and the axial-led inertial modes.

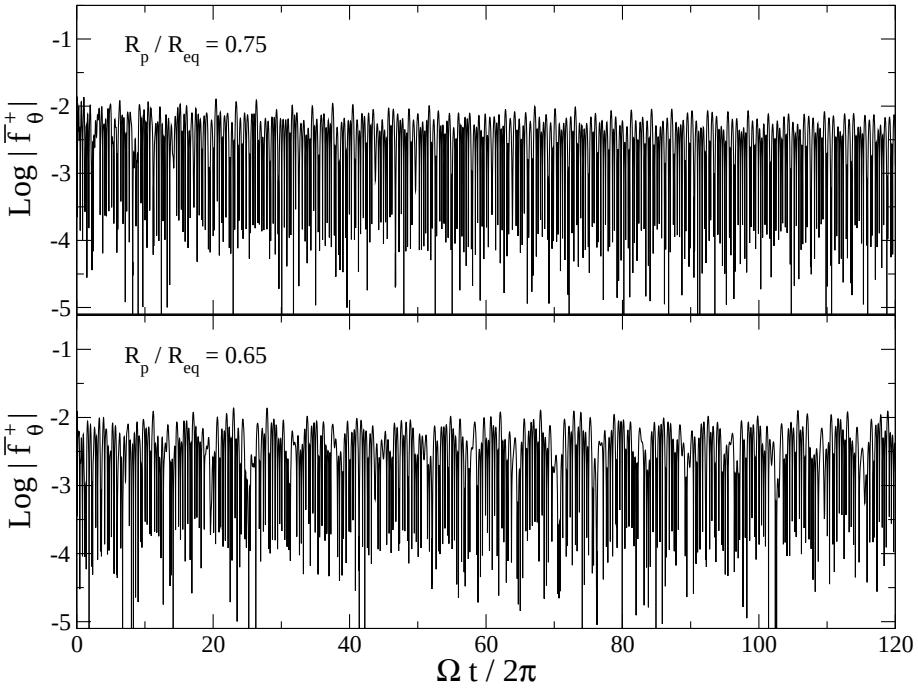

Figure 1. This figure shows the time evolution of the integrated flux component $\bar{f}^{+}_{\theta}$, defined in equation (25), for two fast rotating models with $R_p/R_{eq} = 0.75$ and $R_p/R_{eq} = 0.65$. Time is given in dimensionless units as a number of the star's rotational periods. These two simulations show the stability and the small numerical dissipation of our numerical code.

6 THE CODE

After decomposition with respect to ϕ, the dynamical problem has two spatial dimensions, represented by the angle θ and the new radial coordinate $x = x\,(r, \theta)$. This radial coordinate is fitted to surfaces of constant pressure of the background star and it is normalised to unity on the equatorial radius. The choice of coordinate simplifies the implementation of the surface boundary condition in a perturbed star considerably (Jones et al. 2002). The spatial variables (x, θ) are then discretized on an evenly spaced two-dimensional grid, where $0 \leqslant x \leqslant 1$ and $0 \leqslant \theta \leqslant \pi/2$.

We evolve equations (15)-(17) in time with a Mac-Cormack algorithm, a second order accurate scheme that involves a predictor and a corrector step. In order to prevent spurious numerical oscillations we use a fourth-order Kreiss-Oliger dissipation with a parameter that depends on the numerical grid size. The perturbation equations are evolved for the internal points of the numerical grid, while boundary conditions are used to update the perturbations at the origin, the rotation axis, the surface and the equator. In order to use the fourth-order Kreiss-Oliger dissipation also near the grid boundary one ghost point is added to each grid slice. Numerical simulations are then carried out on (x, θ) grids with 60×32 points. Test simulations on finer grids with 60×64 or 120×32 points do not give significant improvements on the results. The numerical evolutions are stable for several hundred rotation periods. We extract the required mode frequencies from the evolutions by performing a Fast Fourier Transformation (FFT) of the time series of the perturbations.

In order to have global information of the pulsations of the star, the perturbation variables can be integrated on the spatial grid (using a two dimensional integral). For instance, the integrated flux perturbation component f^{+}_{θ} is given by

$$\bar{f}^{+}_{\theta} \equiv \int_0^{\pi/2} d\theta \int_0^{R(\theta)} f^{+}_{\theta}\, r dr\,, \tag{25}$$

where $R(\theta)$ is the radius of the star at any angle θ. This integrated quantity is shown in Fig 1, for two fast rotating stellar models with axis ratio 0.75 and 0.65, for evolutions lasting up to 120 rotation periods. This figure illustrates the codes stability as well as the very small numerical dissipation. Similar characteristics are observed for other perturbation quantities. These results demonstrate a significant improvement on the results reported in Jones et al. (2002). This improvement in stability allows us to analyse correspondingly longer stretches of data, providing more accurate localisation of modes in frequency space.

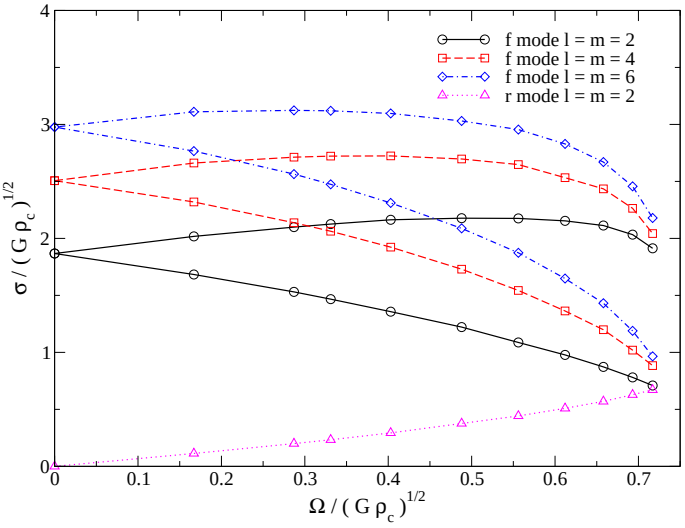

Figure 2. This figure displays the frequencies of the $l = m$ f- and r-modes as a function of the rotating rate for the $\Gamma_\beta = 2$ barotropic sequence of rotating stars. The mode frequencies are determined in the rotating frame. All frequencies are given in units of $\sqrt{G\rho_c}$, where ρ_c is the mass density at the stellar centre. These results test our numerical code in the limit of barotropic stars. The mode frequencies are in good agreement with those reported by Jones et al. (2002).

7 RESULTS

7.1 Initial Data

Once we fix the azimuthal harmonic index m the code evolves linear oscillations on an axisymmetric background. This means that modes with any value of l can be excited. This makes the problem different from a perturbation analysis in the frequency domain, where one tends to have some control over the specific angular dependence of the modes that are studied. The spectral content of the evolutions, which is extracted from an FFT of the time evolved perturbation variables, depends on the initial data used to excite the motion.

On the initial time slice, a single oscillation mode can, in principle, be excited by providing the correct eigenfunctions for the perturbation variables. However, this is not a practical strategy since it requires the mode-problem to be solved already. An alternative is to use an eigenfunction recycling method (Stergioulas et al. 2004; Dimmelmeier et al. 2006). In this study we do not need these refinements. We are interested in a multi-mode analysis, so we can simply choose arbitrary initial perturbations that excite as many modes as possible in a single numerical simulation.

We excite type I parity perturbations with a Gaussian radial profile in the pressure perturbation:

$$\delta P = \rho \, \exp\left[- \left(\frac{r - r_0}{q R\left(\theta\right)} \right)^2 \right] Y_{ll}\left(\theta, \phi\right) \, , \tag{26}$$

where $R\left(\theta\right)$ is the stellar radius at polar angle θ, and the parameters r_0 and q determine the centre of the Gaussian and its width, respectively. The function $Y_{ll}\left(\theta, \phi\right)$ is the $l = m$ spherical harmonic which describes a typical polar mode angular pattern of a spherical star. The initial conditions of the mass flux $\mathbf{f}$ and proton fraction $\chi_{\rm P}$ perturbations are set to zero. Type II parity perturbations are instead excited by the flux perturbation:

$$\mathbf{f} = \rho \, \exp\left[- \left(\frac{r - r_0}{q R\left(\theta\right)} \right)^2 \right] Y^B_{ll}\left(\theta, \phi\right) \, , \tag{27}$$

where $Y^B_{ll}\left(\theta, \phi\right)$ is a magnetic spherical harmonic (Thorne 1980). In this case, the pressure and the proton fraction perturbations both vanish on the initial time slice. Note that for both type I and type II parity, the coupling of the perturbed quantities in equations (15)–(17) ensures these these simple choices of initial data sets do in fact excite non-trivial perturbations in all quantities.

7.2 The Barotropic Case

We first consider the problem for barotropic stars. This serves as a useful test-case for the reliability of our evolutions. The results also illustrate the improvements that we have made on the previous analysis (Jones et al. 2002).

In barotropic rotating stars the oscillation spectrum is formed by pressure, fundamental and inertial modes. Rotation removes the degeneracy (in m) of the non-axisymmetric pressure and f-modes and generates the new family of inertial modes,

Table 2. Inertial mode frequencies for barotropic rotating models with $\Gamma_\beta = 2$. The purely axial $l = m = 2$ r-mode is denoted by the symbol ${}^l\mathrm{r}$ and the inertial modes by ${}^l\mathrm{i}_\mathrm{k}$, where k labels different modes with the same l. The second column shows the overall mode parity, i.e. whether the mode is axial or polar-led. Frequencies determined by Lockitch & Friedman (1999) are labeled with the acronym L-F and listed in the third column, while those extracted from our numerical code are shown in the last two columns for two slowly rotating models. In the formalism used by L-F, positive and negative eigenfrequencies correspond to counter and co-rotating modes respectively. In an FFT of a time evolved perturbation variable, they all appear positive, but their counter- or co-rotating character can easily be established by comparison with the L-F results and the dependence on the rotation of the star.

Mode	Parity	σ/Ω L-F	σ/Ω $R_p/R_{eq} = 0.983$	σ/Ω $R_p/R_{eq} = 0.95$
${}^2\mathrm{r}$	a	0.667	0.676	0.695
${}^3\mathrm{i}_1$	p	-0.557	0.562	0.549
${}^3\mathrm{i}_2$	p	1.100	1.101	1.116
${}^4\mathrm{i}_1$	a	-1.026	1.021	1.036
${}^4\mathrm{i}_2$	a	0.517	0.508	0.536
${}^4\mathrm{i}_3$	a	1.358	1.363	1.375
${}^5\mathrm{i}_1$	p	-1.273	1.291	1.296
${}^5\mathrm{i}_2$	p	-0.275	0.252	0.258
${}^5\mathrm{i}_3$	p	0.863	0.834	0.884
${}^5\mathrm{i}_4$	p	1.519	1.512	1.519
${}^6\mathrm{i}_1$	a	0.422	0.391	0.409

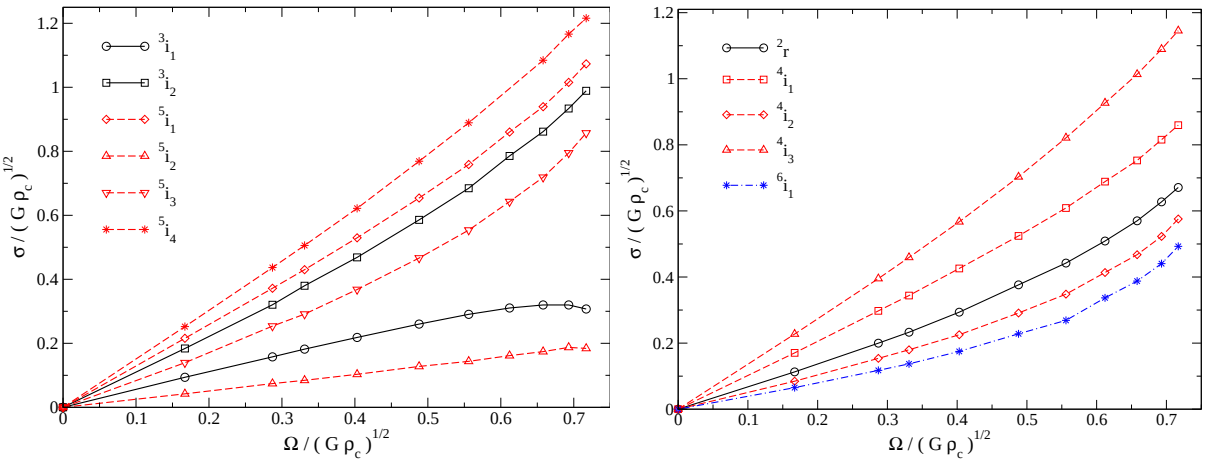

Figure 3. Rotating frame frequencies of polar-led inertial modes (left panel) and the r-mode and other axial-led inertial modes (right panel) as a function of the rotation rate for $\Gamma_\beta = 2$ barotropic models. The inertial mode frequencies shown in this figure reproduce with good accuracy the results presented by Jones et al. (2002). In the limit of slow rotation, the mode frequencies are also in good agreement with the results reported by Lockitch & Friedman (1999), see Table 2.

which are restored by the Coriolis force. The main properties of the inertial modes are that they vanish linearly in the limit of zero stellar rotation and that they have mixed nature. Even in the slow rotation limit the velocity perturbations of the inertial modes have both axial and polar parts (Lockitch & Friedman 1999). However, one can still identify two independent classes of inertial modes. The axial-led class with parity $(-1)^{m+1}$ and the polar-led modes with parity $(-1)^m$. The velocity perturbation of an axial-led inertial mode can couple only with axial terms having $l = m, m+2, \ldots$ and with polar terms having $l = m+1, m+3, \ldots$. In the case of a polar-led inertial mode, the velocity perturbation couples only with $l = m, m+2, \ldots$ polar terms and $l = m+1, m+3, \ldots$ axial terms. A particular subset of the axial-led inertial modes is formed by the r-modes, which have purely axial velocity perturbations in the slow-rotation limit. For barotropic stars only $l = m$ r-modes can exist.

The non-axisymmetric modes of barotropic Newtonian rotating stars have been extensively investigated in literature. We tested our numerical code by reproducing the results of the previous code developed by Jones et al. (2002), finding a very good agreement. For stars with $\Gamma_\beta = \Gamma_\mathrm{f} = 2$, we show in Fig. 2 the rotational splitting of the $l = m$ f-modes and the $l = m = 2$ r-mode. The final stellar model in the sequence is rotating very fast, at about 99 percent of the Kepler limit. The new code performs significantly better that the one discussed in Jones et al. (2002). In particular, the improved stability allows us to study configurations that rotate closer to the break-up limit. Being able to carry out longer simulations, we can also improve on the precision of the extracted mode frequencies.

In addition to the f-mode, many inertial modes are excited during a typical evolution. For type I parity perturbations

Table 3. Comparison of the first two $l = 2, 3, 4$ g-modes frequencies with the Yoshida & Lee (2000) results. The star is non-rotating and have adiabatic indices $\Gamma_\beta = 2$ and $\Gamma_{\rm f} = 2.0004$. The frequencies are given in units of $\sigma/\sqrt{G\rho_c}$ and the Yoshida and Lee values are denoted with YL.

l	g_1 YL	g_1	g_2 YL	g_2
2	0.0189	0.0187	0.0129	0.0123
3	0.0227	0.0229	0.0162	0.0159
4	0.0255	0.0252	0.0189	0.0188

Table 4. The frequencies of the first three $l = 2$ g-modes for a non-rotating non-barotropic model with $\Gamma_\beta = 2$ and three different values of $\Gamma_{\rm f} = 2.05, 2.2, 2.4$. The frequencies are given in units of $\sigma/\sqrt{G\rho_c}$. This comparison of modes determined with a frequency (FD) and time domain (TD) approach provide a useful reliability check of our time evolutions.

$\Gamma_{\rm f}$	${}^2g_1$ FD	${}^2g_1$ TD	${}^2g_2$ FD	${}^2g_2$ TD	${}^2g_3$ FD	${}^2g_3$ TD
2.05	0.195	0.208	0.134	0.141	0.102	0.111
2.2	0.383	0.396	0.266	0.271	0.205	0.209
2.4	0.531	0.530	0.370	0.367	0.287	0.284

and $m = 2$, we can identify polar-led $l = 3$ and $l = 5$ inertial modes. These are shown in the left panel of Fig. 3 for several barotropic rotating stars. For $m = 2$ type II parity initial conditions, axial-led $l = 4$ and $l = 6$ inertial modes and the $l = m = 2$ r-mode are excited and their frequencies are shown in the right panel of Fig. 3. In order to identify and test the inertial mode frequencies, we have compared them to the frequencies determined by Lockitch & Friedman (1999). As is clear from the data in Table 2, the agreement is better than 6% for slowly rotating barotropic models with axis ratio $R_p/R_{eq} = 0.983$ and $R_p/R_{eq} = 0.95$.

It is worth noting that, some of the eigenfrequencies in Table 2 are negative as these modes are co-rotating with the stellar fluid. Meanwhile, the frequencies that we extract will always be positive, as we are using an FFT of the time evolved perturbations. The co- and counter-rotating character of the various modes can be established by comparison with the results determined by Lockitch & Friedman (1999). In some cases, the nature of the mode can also be inferred from the dependence on the rotation rate of the star. As can be seen from, for example, Figure 3 some of the co-rotating mode frequencies (in the rotating frame) tend to decrease at fast rotation rates. Meanwhile, no counter-rotating modes show this effect.

7.3 Stratified Stars

The oscillation spectrum of a stratified star is, in a sense, richer than that of a barotropic model. Fluid elements that have moved away from the equilibrium position can produce composition gradients in the stellar matter. For small displacements, buoyancy acts as restoring force by producing an oscillatory motion of the perturbed fluid element. These oscillation modes are called composition gravity modes (g-modes). They must been discerned from thermal g-modes, which are due to temperature gradients. The latter are only relevant in newly born neutron stars, while the composition modes are relevant also in mature systems. Gravity modes have a polar nature, appear in the low-frequency band of the oscillation spectrum, typically around 100 Hz, and exist even for non-rotating stellar models. Like f- and p-modes, each g-mode can be labeled by the harmonic indices l and m together with the number of nodes in the radial eigenfunction. We will label individual g-modes using the notation ${}^l g_{\rm k}$, where k labels different modes sharing the same value of the index l. Additionally, we will denote a retrograde (as opposed to prograde) mode as ${}^l g^{\rm r}_{\rm k}$

There is an overlap in frequency space between the g-modes and the inertial modes. In fact, since both sets of modes emerge from the degenerate trivial modes of a non-rotating barotropic model, one might expect them to be intimately related. In order to understand this relationship better, we will investigate the low frequency oscillations of non-barotropic rotating neutron stars. The aim is to clarify whether inertial and g-modes are both present in the spectrum and to what extent it is possible to distinguish them. We also want to understand their behaviour in fast rotating models.

These issues can be directly related to the dynamics of a perturbed fluid element and the balance between the two restoring forces that are acting on it, the Coriolis and the buoyancy force. In slowly rotating and stratified neutron stars with large composition gradients, buoyancy is expected to dominate the Coriolis force. As a result, a typical mode should appear as a g-mode. For higher rotation rates, the effect of the Coriolis force increases and may dominate the buoyancy force beyond a given stellar spin. In this regime, the oscillation mode should behave as an inertial mode. The threshold between these two

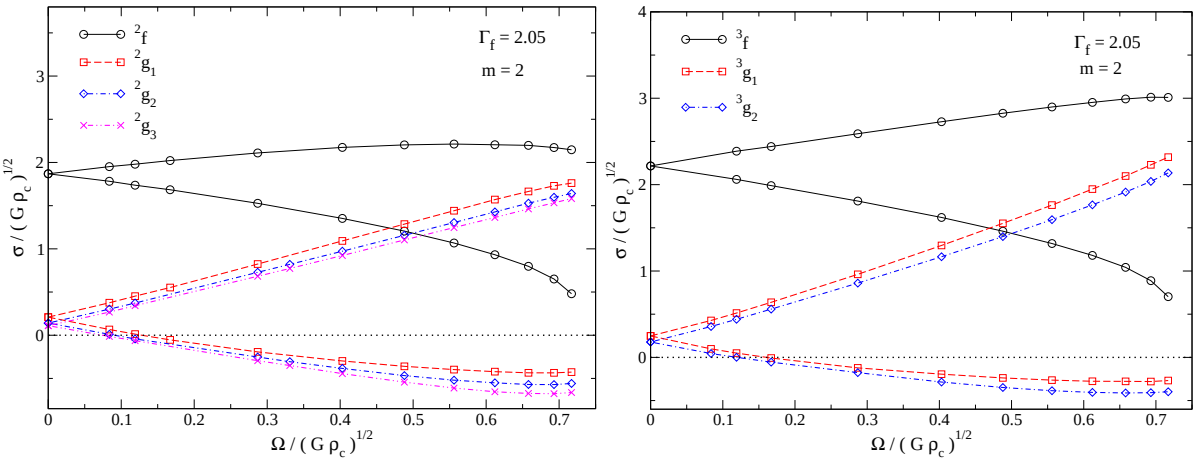

Figure 4. Results for non-barotropic rotating stellar models with $\Gamma_\beta = 2$ and $\Gamma_f = 2.05$. The left panel shows the frequencies of the $l = m = 2$ f- and g-modes, while the right panel shows the corresponding modes for $l = 3$ and $m = 2$. In order to emphasize the rotational splitting of the g-modes and the onset of the CFS instability, the frequencies are shown in the reference frame of an inertial observer.

regimes depends on the magnitude of the composition gradient and must obviously be smaller than the mass shedding limit of the star to be of any interest.

The order of magnitude of the composition g-mode frequencies can be estimated by the Brunt-Väisälä frequency N, which is defined by (see e.g., Unno et al. 1989)

$$N^2 \equiv \frac{\nabla P}{\rho} \cdot \mathbf{A} = \left(\frac{1}{\Gamma_\beta} - \frac{1}{\Gamma_f} \right) \frac{|\nabla P|^2}{\rho P} \,. \tag{28}$$

For non-rotating stars this frequency can be written

$$N^2 = -gA = -g \left(1 - \frac{\Gamma_\beta}{\Gamma_f} \right) \frac{d \ln \rho}{dr} \,, \tag{29}$$

where the equilibrium configuration equations have been used to replace the pressure gradient with the gravitational acceleration. An averaged value of equation (29) can be estimated by approximating the gravitational acceleration as $g \simeq GM/R^2 \simeq (4\pi/3)\, GR\langle\rho\rangle$, where $\langle\rho\rangle$ is the mass density average, and the density gradients as $d\rho/dr \simeq -\rho_c/R$. As a result, the averaged and dimensionless Brunt-Väisälä frequency $\hat{N} \equiv N/\sqrt{G\rho_c}$ is given by:

$$\langle \hat{N} \rangle \simeq \sqrt{\frac{4\pi}{3}} \left(1 - \frac{\Gamma_\beta}{\Gamma_f} \right)^{1/2} \,. \tag{30}$$

We have tested equation (30) with the average of equation (28) for the non-rotating and non-barotropic models used in this paper. The results agree to better than 5%.

We want to study the effects of composition gradients on the spectrum in detail. We consider non-barotropic models with $\Gamma_\beta = 2$ and frozen composition indices between $\Gamma_f = 2.05$ and $\Gamma_f = 2.4$ in order to investigate stars with low and high composition gradients. It is useful to begin by estimating at what rotation rate the Coriolis force will start to dominate the buoyancy. When $\Gamma_f = 2.05$, equation (30) suggests that $N \sim 2\Omega$ for a model with $\Omega/\sqrt{G\rho_c} = 0.16$. For models rotating much faster than this, we would expect the Coriolis force to dominate. As a result, one would expect the low-frequency modes of such models to have a predominantly inertial character. As we will see later, the trend suggested by this rough estimate is brought out by the detailed mode-calculations.

The non-barotropic evolution code has been tested against two eigenvalue codes developed by Yoshida & Lee (2000) and Passamonti, Stavridis & Kokkotas (2008), respectively. Yoshida & Lee (2000) solve for linear perturbations of slowly rotating neutron stars in Newtonian gravity, whereas Passamonti et al. (2008) study the pulsation spectra of slowly rotating relativistic stars in the Cowling approximation. We have compared the first two g-modes frequencies with the non-rotating and weakly stratified Newtonian model of Yoshida & Lee (2000), which has $\Gamma_\beta = 2$ and $\Gamma_f = 2.0004$. The relevant frequencies, which are given in Table 3, show a very good agreement even though we are using the Cowling approximation. The second $l = 2$ g-mode have an error of four percent, while the others are accurate to within two percent. This difference is due the low frequency of the second $l = 2$ g-mode that requires a longer time evolution for extracting a more accurate value with an FFT.

We have further tested our code on neutron star models with larger composition gradients by using the Passamonti et al. (2008) code. Since the time evolution code used in this paper is Newtonian, we have made a comparison between the two codes for a spherically symmetric background model with low compactness. For a polytropic model with $\Gamma_\beta = 2$ and a star with central density $\rho_c = 4.5 \times 10^{14}$ g cm^{-3}, the Tolman-Oppenheimer-Volkoff equations determine a non-rotating star with mass $M = 1.17 M_\odot$ and radius $R = 16$ km, giving a compactness ratio of $M/R = 0.11$. In terms of the dimensionless quantity

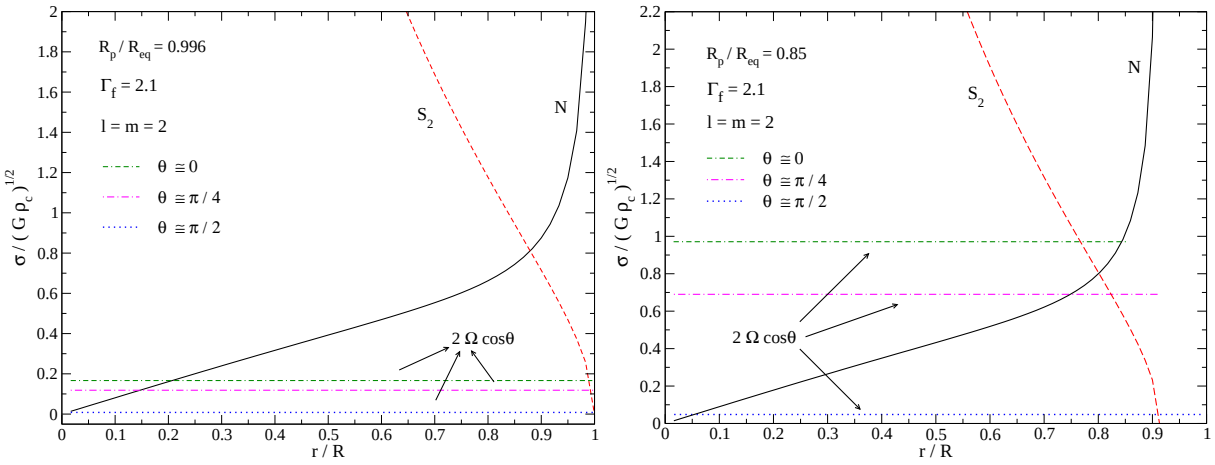

Figure 5. This figure displays the propagation diagram of two stratified models with $\Gamma_{\rm f} = 2.1$ and $\Omega/\sqrt{G\rho_c} = 0.084$ in the left panel and $\Omega/\sqrt{G\rho_c} = 0.488$ in the right panel. The Brunt-Väisälä frequency N, the Lamb frequency S_l and the Coriolis term $2\Omega\cos\theta$ of the dispersion relation (32) are given in $\sqrt{G\rho_c}$ units. On the horizontal-axis the radial coordinate r is normalized with the stellar radius R. For simplicity, the N and S_l frequencies are presented in the two panels for $\theta = \pi/4$, while three directions are shown for the Coriolis term, respectively $\theta = 0, \pi/4$ and $\pi/2$. The two propagation diagrams illustrate the regions of the star where the various restoring forces dominate. Increasing the stellar spin, the Coriolis term becomes stronger than the Brunt-Väisälä frequency in almost all the volume of the star. Only in a small region near the equator, buoyancy can dominate even in rapidly rotating stars.

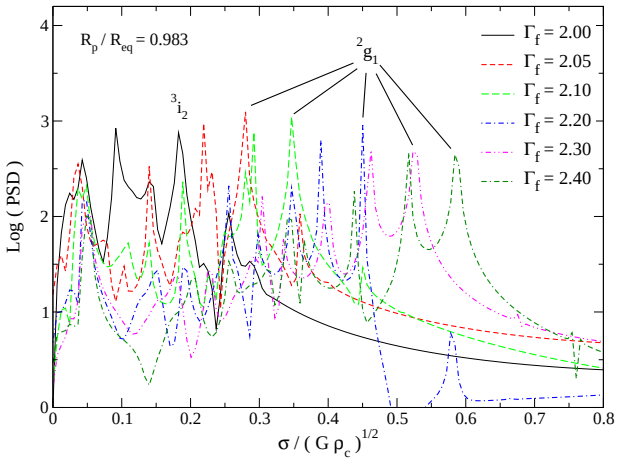

Figure 6. This figure shows the Power Spectral Density (PSD) of the integrated flux perturbation component f_θ^+ for a set of slowly rotating barotropic and non-barotropic models. All these models have axis ratio $R_p/R_{eq} = 0.983$ (corresponding to $\Omega/\sqrt{G\rho_c} = 0.167$), but different frozen composition adiabatic index $\Gamma_{\rm f}$. The solid line corresponds to a barotropic star with $\Gamma_{\rm f} = 2$. The counter-rotating ${}^2{\rm g}_1$ mode has been determined, from left to right in the figure, for stars with $\Gamma_{\rm f} = 2.05, 2.1, 2.2, 2.3, 2.4$. This figure shows the dependence of the ${}^2{\rm g}_1$ mode frequency on the composition gradients. In the limit of $\Gamma_{\rm f} \to \Gamma_\beta$, the counter-rotating ${}^2{\rm g}_1$ mode seems to approach the ${}^3{\rm i}_2$ inertial mode. This behaviour is clearer in Fig (7).

used in our time domain code, this model has $M/\left(\rho_c R^3\right) = 1.262$ which agrees very well (within one percent) with the non-rotating model in Table 1. By using these two approaches, we determined the g-mode frequencies of non-rotating stratified neutron stars in Table 4. For non-barotropic stars with $\Gamma_{\rm f} = 2.05$ the frequencies of the first three modes agree to better than eight percent, while for $\Gamma_{\rm f} = 2.4$ they agree to better than one percent. This level of agreement is satisfactory given that the calculations are carried out within completely different frameworks. Thus we are confident that our time-evolutions are able to provide accurate g-mode results.

The rotational splitting of the $l = m = 2$ f- and g-modes for stratified stars with $\Gamma_{\rm f} = 2.05$ is shown, in the frame of an inertial observer, in Fig. 4. The left panel represents modes with type I parity, while the right panel shows results for type II parity. The two classes of modes clearly behave in a similar fashion. Results for other values of $\Gamma_{\rm f}$ are similar. Generally, we observe that the frequencies of the f- and g-modes tend to increase for stars with larger composition gradients, i.e. larger $\Gamma_{\rm f}$. From the results in Fig. 4 it is easy to read off when the low-order g-modes become susceptible to the gravitational-radiation driven CFS instability (Friedman & Schutz 1978; Andersson 2003). The instability condition is that the mode-frequency

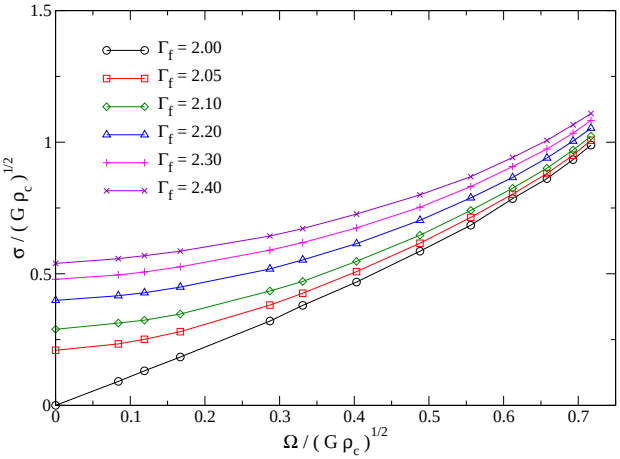

Figure 7. This figure displays the variation of the counter rotating ${}^2\mathrm{g}_1^{\mathrm{r}}$ mode with the adiabatic index Γ_{f} for a sequence of rotating stellar models. The polar-led inertial mode ${}^3\mathrm{i}_2$ frequencies of the barotropic models with $\Gamma_{\mathrm{f}} = 2$ are shown as a circle-solid line. This figure suggests that in rapidly rotating stars the counter rotating ${}^2\mathrm{g}_1^{\mathrm{r}}$ mode behaves similarly to the barotropic ${}^3\mathrm{i}_2$ inertial mode. This is expected when the rotation rate is larger than the Brunt-Väisälä frequency N, namely $2\Omega > N$, and the Coriolis force starts to dominate over the buoyancy force.

changes sign according to an inertial observer. The results in the figure suggest that this happens for $\Omega/\sqrt{G\rho_c} \approx 0.12$. This is in accordance with the typical values expected for the g-mode CFS instability.

In fact, we can compare our result to an order of magnitude estimate based on the result of Lai (1999). He estimates that the rotation rate of the g-mode instability onset corresponds to

$$\Omega = 0.68\,\sigma_0\,, \tag{31}$$

where σ_0 is the g-mode frequency for the non-rotating model. From this we find that one would expect the instability of the ${}^2\mathrm{g}_1$ mode for the $\Gamma_{\mathrm{f}} = 2.05$ model to be triggered in a star rotating at $\Omega/\sqrt{G\rho_c} \approx 0.14$. This is close to the (presumably more accurate) value determined with our numerical code.

However, the g-mode instability is not thought to be very important since the g-modes are not radiating gravitational waves efficiently. Viscosity is expected to suppress the instability in more realistic models. In comparison, the f-mode, which radiates gravitational waves efficiently does not go unstable until the star spins extremely fast. For stellar models with $\Gamma_\beta = 2$, the $l = m = 2$ f-mode is not expected to become unstable before the mass shedding limit rotational rate is reached (Ipser & Lindblom 1990). As is clear from Fig. 4, the f-mode instability point occurs for faster spins than we are able to study. This accords well with previous results in the literature.

Let us now study the low frequency band of rotating non-barotropic stars. A local analysis of uniformly rotating stars in the Cowling approximation leads to the following dispersion relation for low-frequency waves (Unno et al. 1989):

$$\sigma^2 \simeq \frac{N^2 k_\perp^2 + (2\mathbf{\Omega}\cdot\mathbf{k})^2}{k^2}\,, \tag{32}$$

where $\mathbf{k}$ is the wave vector and $k_\perp$ is its component orthogonal to the apparent gravity. These modes are generally referred to as inertia-gravity waves by Unno et al. (1989), as they are restored by both gravity and the Coriolis force. In the barotropic case, $N = 0$, equation (32) describes the inertial waves, while for a non-rotating model it reduces to the usual gravity waves. In stratified and rotating neutron stars, it is thus to be expected that the low-frequency oscillation modes have an hybrid character with gravity dominating at low rotation rates and the Coriolis force taking over at fast stellar spin.

However, it is worth noting that the buoyancy and the Coriolis force can be locally dominant in different regions of the star. This can be understood from a propagation diagram that illustrates the spectral properties of the star. For instance, we consider two stellar models with frozen adiabatic index $\Gamma_{\mathrm{f}} = 2.1$ and with angular velocity $\Omega/\sqrt{G\rho_c} = 0.084$ and $\Omega/\sqrt{G\rho_c} = 0.488$, respectively. For these models we determine the Brunt-Väisälä frequency N (28), the Lamb frequency (Unno et al. 1989)

$$S_l^2 = \frac{l\,(l+1)}{r^2} c_s^2\,, \tag{33}$$

and effect of the Coriolis force on the dispersion relation (32), i.e. $2\Omega\cos\theta$. The role of the Lamb frequency is to estimate the propagation region for acoustic modes. For these two stellar models, the propagation diagram for the $l = m = 2$ modes is shown in Fig. 5 using the normalized radial coordinate r/R. For the slowly rotating star with $R_p/R_{eq} = 0.996$, the N and S_l frequencies do not vary much, while the effect of the Coriolis force term $2\Omega\cos\theta$ changes according to its angular dependence, from zero at the equator to the maximum at the pole. In this case, the star is spinning so slowly that the buoyance (N) is dominant in most of the star. Only near the centre, for $r \lesssim 0.2R$, is the Coriolis force stronger. As a result, we should expect the inertia-gravity modes to behave as g-modes. Later, this will be confirmed by a global mode analysis. When the

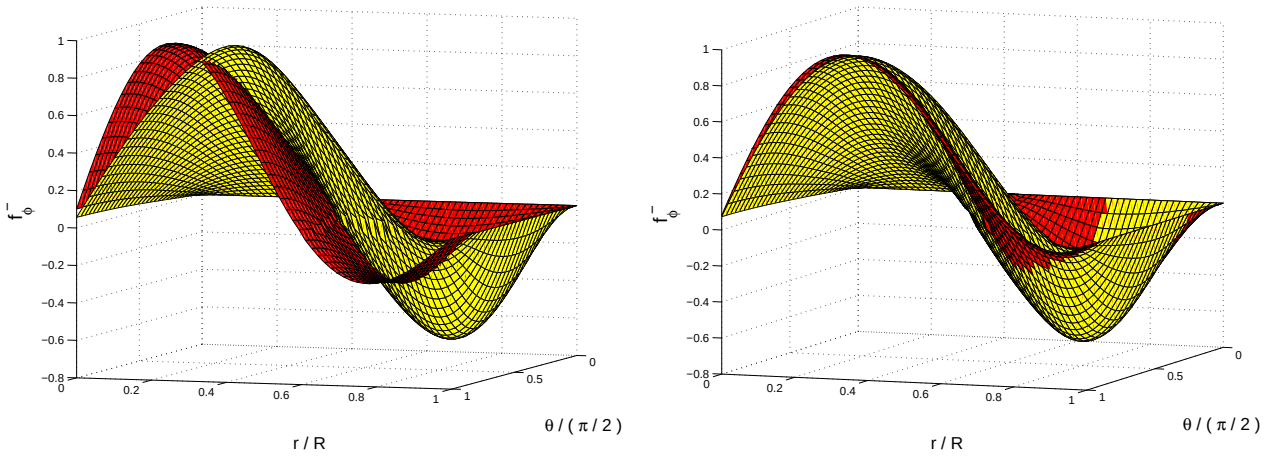

Figure 8. Eigenfunctions of the flux component perturbation f_ϕ^- for rotating stellar models with rotation rate $\Omega/\sqrt{G\rho_c} = 0.084$ (left panel) and $\Omega/\sqrt{G\rho_c} = 0.488$ (right panel). The yellow surfaces refer to the ${}^3\mathrm{i}_2$ inertial mode of barotropic models with $\Gamma_\mathrm{f} = \Gamma_\beta = 2$, while the red surfaces represent the counter-rotating ${}^2\mathrm{g}_1^\mathrm{r}$ mode of stratified stars with $\Gamma_\mathrm{f} = 2.1$ and $\Gamma_\beta = 2$. This figure illustrates how g- and inertial mode eigenfunctions become similar for increasing rotation rates.

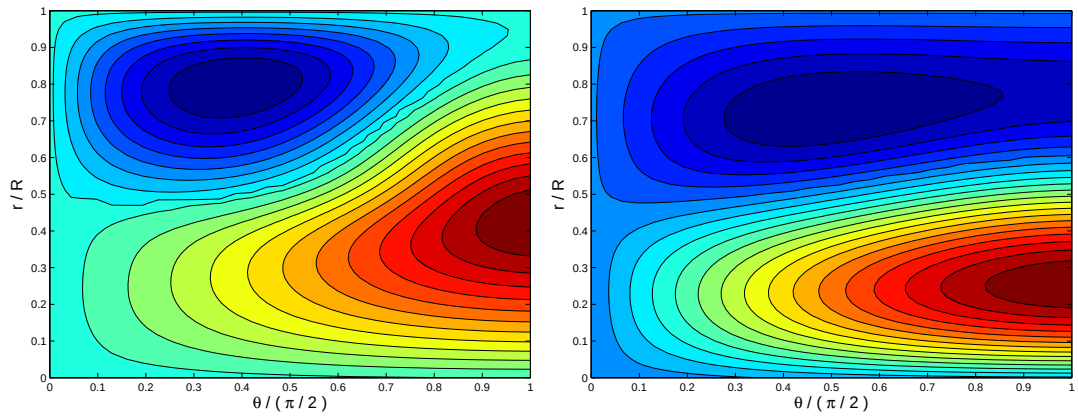

Figure 9. Eigenfunctions of the flux component perturbation f_ϕ^- for the rotating stellar model with rotation rate $\Omega/\sqrt{G\rho_c} = 0.084$. The left panel shows the contour plot of the ${}^3\mathrm{i}_2$ inertial mode for the barotropic model with $\Gamma_\mathrm{f} = \Gamma_\beta = 2$. The right panel displays the contour plot of the counter-rotating ${}^2\mathrm{g}_1$ mode of a stratified star with $\Gamma_\mathrm{f} = 2.1$ and $\Gamma_\beta = 2$. These plots give a complementary view of the eigenfunctions shown in the left panel of Fig. (8), and confirm the difference between the two modes in a slowly rotating model.

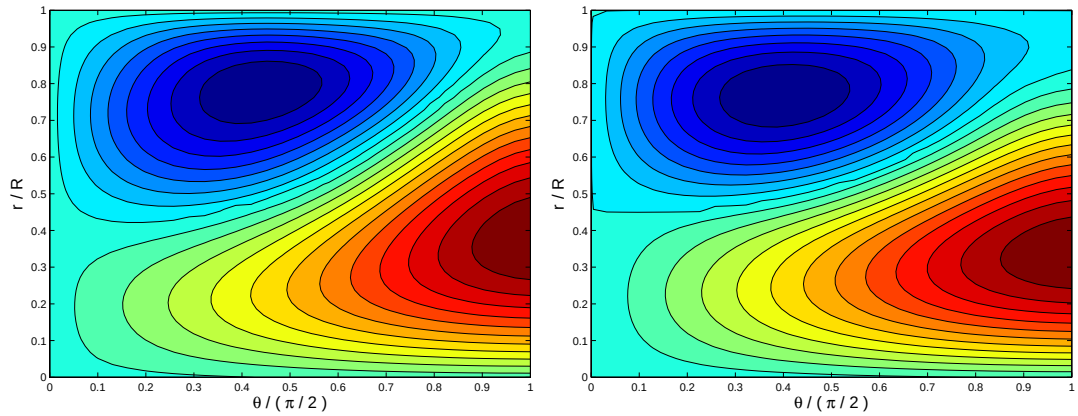

Figure 10. Eigenfunctions of the flux component perturbation f_ϕ^- for the rotating stellar model with rotation rate $\Omega/\sqrt{G\rho_c} = 0.488$ The left panel shows the contour plot of the ${}^3\mathrm{i}_2$ inertial mode for the barotropic model with $\Gamma_\mathrm{f} = \Gamma_\beta = 2$. The right panel displays the contour plot of the counter-rotating ${}^2\mathrm{g}_1$ mode of a stratified star with $\Gamma_\mathrm{f} = 2.1$ and $\Gamma_\beta = 2$. These plots confirm the results of Fig. (8) showing that the structure of these two eigenfunctions becomes similar in fast rotating models.

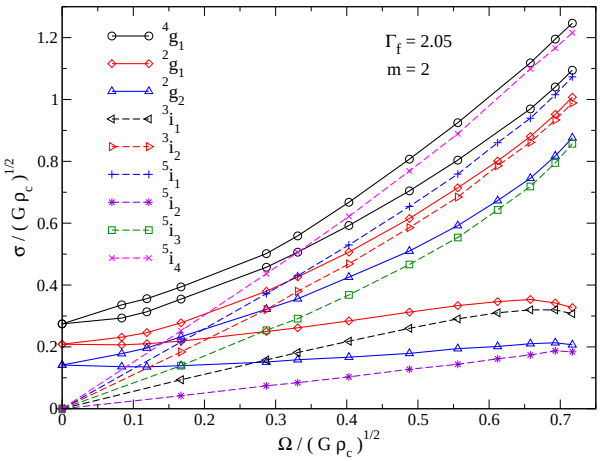

Figure 11. Frequencies of some selected g-modes (solid lines) for $\Gamma_{\rm f} = 2.05$ models and polar-led inertial modes (dashed lines) of the barotropic $\Gamma_\beta = \Gamma_{\rm f} = 2$ model. All frequencies are measured in the rotating frame. The dominance of the Coriolis force in rapidly rotating stars is evident from this figure. We see that the g-modes are mainly restored by the Coriolis force when $\Omega/\sqrt{G\rho_c} > 0.3$, and thus become similar to the barotropic inertial modes.

star rotates faster, as in the model with $R_p/R_{eq} = 0.85$ (right panel of Fig. 5), the Coriolis term is more important and larger than the Brunt-Väisälä frequency in the most of the star. In order to keep the figure clear, we have shown the N and S_l frequencies only for $\theta = \pi/4$. The change in the other directions is visible, but does not modify the qualitative properties of the propagation diagram. However, even in weakly stratified and rapidly rotating stars there is a region near the equator where buoyancy dominates over the Coriolis force. This region, which is due to the $\cos\theta$ dependence of the Coriolis term, shrinks for higher rotation rates.

The inertia-gravity modes can be identified in our time domain simulations by studying the FFT of the perturbation evolution and extracting the 1D and 2D mode eigenfunctions with the code developed by Stergioulas et al. (2004) and Dimmelmeier et al. (2006). In order to study the dependence of the modes on the stellar spin and stratification, we construct a set of equilibrium models by gradually varying the two parameters Ω and $\Gamma_{\rm f}$. We can then follow the change of the mode frequency and eigenfunction shape and correctly distinguish it among the other peaks in the spectrum. Let us consider, for instance, a sequence of slowly rotating models with fixed rotation rate $\Omega/\sqrt{G\rho_c} = 0.167$ and different $\Gamma_{\rm f}$. Typical FFT results are shown in Fig. 6, where we have identified the $^3{\rm i}_2$ inertial mode for the barotropic model and the counter-rotating $^2{\rm g}_1^{\rm r}$ mode for a set of stars with increasing composition gradients. The results suggest that the g-mode frequency approaches the barotropic inertial mode in the limit $\Gamma_{\rm f} \to 2$. This association becomes more evident if we combine these results for a set of rotating models, see Fig. 7. When the star rotates with $2\Omega \gtrsim N$, the retrograde $^2{\rm g}_1^{\rm r}$ mode seems to behave as the barotropic $^3{\rm i}_2$ inertial mode. This transition obviously depends on the level of stratification. This property is also noted in the mode eigenfunctions. In Figs. 8–10, we show how the eigenfunctions of the mass flux component f_ϕ^- of the counter-rotating $^2{\rm g}_1^{\rm r}$ mode approach the shape of the $^3{\rm i}_2$ mode when $2\Omega > N$. In this case, the non-barotropic star has $\Gamma_{\rm f} = 2.1$ and an estimated Brunt-Väisälä frequency $\langle N/\sqrt{G\rho_c}\rangle \simeq 0.447$, see equation (30). In Fig. 8 we provide a three-dimensional picture of the eigenfunctions, for rotation rate $\Omega/\sqrt{G\rho_c} = 0.084$ in the left panel, and for $\Omega/\sqrt{G\rho_c} = 0.488$ in the right panel (the latter corresponding to a star with an angular velocity slightly larger than the Brunt-Väisälä frequency). Clearly, for the slower rotation rate (left panel) the f_ϕ^- the $^2{\rm g}_1$ eigenfunction is quite different from the eigenfunction of the barotropic $^3{\rm i}_2$ mode. In particular, the nodal curve of the two modes do not coincide near the equator. In contrast for the more rapidly rotating star (right panel) the nodal curves of the two modes are very similar. This can be seen particularly clearly in the contour plots of the eigenfunctions given in Fig. 9 (for $\Omega/\sqrt{G\rho_c} = 0.084$) and Fig. 10 (for $\Omega/\sqrt{G\rho_c} = 0.488$).

When we extend this approach to the other g and inertial modes, we find further mode associations. Combined results are provided in Figs. 11 and 12. These figures display the spectrum of barotropic models and stratified stars with $\Gamma_{\rm f} = 2.05$. The results show that individual non-barotropic g-modes tend towards specific barotropic inertial modes as the rotation rate of the star is increased. This agrees with the notion that the Coriolis force dominates the buoyancy in fast spinning systems. From the results in the two figures we can identify various g-modes with barotropic inertial-mode counterparts. For type I parity and $m = 2$ this leads to:

$$^4{\rm g}_1^{\rm r} \longleftrightarrow {}^5{\rm i}_4, \qquad ^4{\rm g}_1^{\rm p} \longleftrightarrow {}^5{\rm i}_1, \qquad ^2{\rm g}_1^{\rm r} \longleftrightarrow {}^3{\rm i}_2, \qquad ^2{\rm g}_1^{\rm p} \longleftrightarrow {}^3{\rm i}_1, \qquad ^2{\rm g}_2^{\rm r} \longleftrightarrow {}^5{\rm i}_3, \qquad ^2{\rm g}_2^{\rm p} \longleftrightarrow {}^5{\rm i}_2\,, \tag{34}$$

where the upper index r and p denotes retrograde and prograde g-modes respectively. Meanwhile, for type II parity and $m = 2$ we find that:

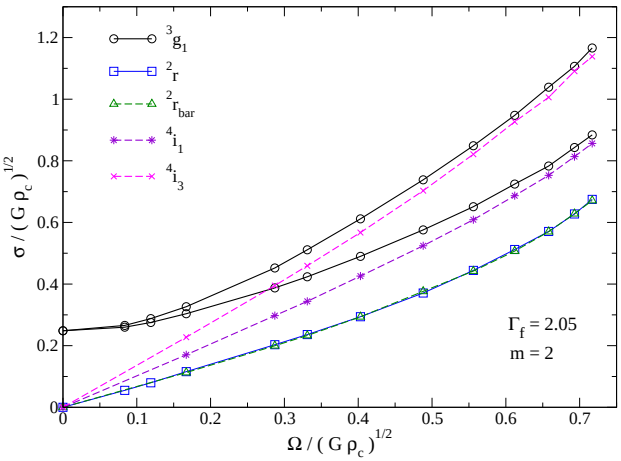

Figure 12. Frequencies of some selected $m = 2$ g-modes (solid lines) for $\Gamma_{\rm f} = 2.05$ models and axial-led inertial modes (dashed line) of the barotropic models $\Gamma_\beta = \Gamma_{\rm f} = 2$. Frequencies are measured in the rotating frame. The counter- and co-rotating $^3g_1$ modes approach the frequencies of the axial-led inertial modes in the limit of fast rotation. In contrast, the r-mode is essentially unaffected by composition gradients.

$$^3g_1^{\rm r} \longleftrightarrow {}^4i_3\,, \qquad {}^3g_1^{\rm p} \longleftrightarrow {}^4i_1\,. \tag{35}$$

From Fig. 12 we also see that it is only the $l = m$ r-mode that does not have a g-mode counterpart. As expected, the r-mode is essentially the same in the barotropic and non-barotropic models. In the type II parity perturbations we could accurately determine only the first g-mode, as the r-mode peak was dominant in the FFT and overwhelmed the higher order g-modes.

These results are consistent with the study of Yoshida & Lee (2000), where the authors worked within the slow rotation approximation and in the frequency domain. They studied inertia-gravity modes of $\Gamma_\beta = 2$ polytropic models with weak stratification and slow rotation. In fact, their frozen adiabatic index corresponds to $\Gamma_{\rm f} = 2.0004$ and the fastest rotating model they consider represents $\Omega/(GM/R^3)^{1/2} = 0.1$, where M and R are respectively the mass and radius of the non-rotating models. In our units this rotation rate in equivalent to $\Omega/(G\rho_c)^{1/2} = 0.113$ and an axis ratio $R_p/R_{eq} \gtrsim 0.992$. In contrast, in the present work we investigate rapidly rotating models up to $\Omega/(G\rho_c)^{1/2} = 0.717$ ($R_p/R_{eq} = 0.6$) and with larger composition gradients. We have tested our results against those of Yoshida & Lee (2000) by numerically evolving $m = 2$ perturbations of the two slowest rotating models reported in Table 1 with $\Gamma_{\rm f} = 2.0004$. The frequencies have an accuracy to better than 2 percent. Finally, equations (34) and (35) respect the connection rules reported in Yoshida & Lee (2000).

8 CONCLUDING REMARKS

Information concerning the oscillation spectra of realistic neutron star models helps develop our understanding of the physics required to describe these objects. Any spectral property can in principle be attributed to particular physical quantities or configurations of the star. Astero-seismology studies, using either electromagnetic or gravitational signals (or indeed both) may thus help constrain the state of matter at supernuclear densities. Of course, in order to facilitate this, we need to improve our theoretical models and clarify the origin of various stellar pulsation features.

In this paper, we have studied the pulsations of stratified and rapidly rotating neutron stars with the aim of understanding the dependence of the composition g-modes on the rotation rate of the star. The stellar pulsations were studied using the linearised Euler and conservation equations on an axisymmetric background. In order to simplify the problem, we used the Cowling approximation where the gravitational potential perturbations are neglected. This approximation generates only a small error in the g-mode frequencies. The system of perturbation equations was evolved in time by a 2D numerical code based on a standard finite differencing scheme. This code was tested against various results available in literature and demonstrated good accuracy.

Since both Coriolis and buoyancy forces act on a perturbed fluid element of a rotating and stratified star, the low-frequency modes have a mixed inertia-gravity character. They typically behave as g-modes in the slowly rotating limit, while they assume the properties of the inertial modes when the star rotates rapidly. By comparing the oscillation frequencies and the associated eigenfunctions of barotropic inertial modes and the inertia-gravity modes of non-barotropic stars, we have demonstrated how the two sets of modes are associated at fast rotation rates.

Our results show that it would be difficult to deduce the presence of composition gradients from the inertia-gravity mode spectrum of fast rotating stars. However, as the neutron star ages and spins down, the dependence of the inertia-gravity modes

on the star's rotation and their deviation from the inertial barotropic modes can, at least in principle, be used to estimate the Brunt-Väisälä frequency and the degree of stratification.

As an extension of this work, we are currently developing a numerical code for studying the dynamics of rapidly rotating superfluid neutron stars. This is an important development since all mature neutron stars are expected to have superfluid components in the core. It is also well known that the associated multi-fluid dynamics leaves an imprint on the stellar oscillation spectrum, see Lin et al. (2007) for a recent discussion. We hope to be able to report on the initial results of this investigation soon.

ACKNOWLEDGEMENTS

This work was supported by STFC through grant number PP/E001025/1. NA also acknowledges support from STFC via Senior Research Fellowship no PP/C505791/1.

REFERENCES

Andersson N., 2003, Class. Quant. Grav., 20, R105
Andersson N., Comer G., 2007, Living Reviews in Relativity, 10
Andersson N., Kokkotas K. D., 1996, Physical Review Letters, 77, 4134
Andersson N., Kokkotas K. D., 1998, MNRAS, 299, 1059
Andersson N., Kokkotas K. D., 2001, International Journal of Modern Physics D, 10, 381
Arras P., Flanagan É. É., Morsink S. M., Schenk A. K., Teukolsky S. A., Wasserman I., 2003, ApJ, 591, 1129
Benhar O., Ferrari V., Gualtieri L., Marassi S., 2007, General Relativity and Gravitation, 39, 1323
Bildsten L., Ushomirsky G., Cutler C., 1996, ApJ, 460, 827
Carter B., Samuelsson L., 2006, Classical and Quantum Gravity, 23, 5367
Cowling T. G., 1941, MNRAS, 101, 367
Dimmelmeier H., Stergioulas N., Font J. A., 2006, MNRAS, 368, 1609
Dintrans B., Rieutord M., 2000, A&A, 354, 86
Duncan R. C., 1998, ApJ, 498, L45+
Ferrari V., Gualtieri L., 2008, General Relativity and Gravitation, 40, 945
Friedman J. L., Schutz B. F., 1978, ApJ, 222, 281
Hachisu I., 1986, ApJSS, 61, 479
Ipser J. R., Lindblom L., 1990, ApJ, 355, 226
Jones D. I., Andersson N., Stergioulas N., 2002, MNRAS, 334, 933
Kokkotas K. D., Schmidt B., 1999, Living Reviews in Relativity, 2
Lai D., 1999, MNRAS, 307, 1001
Lattimer J. M., Prakash M., 2004, Science, 304, 536
Lattimer J. M., Prakash M., 2007, Phys. Rep., 442, 109
Lin L.-M., Andersson N., Comer G.L., 2008, Phys. Rev. D 78, 083008
Lockitch K. H., Friedman J. L., 1999, ApJ, 521, 764
Papaloizou J. C., Pringle J. E., 1980, MNRAS, 190, 43
Passamonti A., Stavridis A., Kokkotas K. D., 2008, Phys. Rev. D, 77, 024029
Piro A. L., 2005, ApJ, 634, L153
Reisenegger A., Goldreich P., 1992, ApJ, 395, 240
Samuelsson L., Andersson N., 2007, MNRAS, 374, 256
Stergioulas N., Apostolatos T. A., Font J. A., 2004, MNRAS, 352, 1089
Tassoul J.-L., 1978, Theory of rotating stars. Princeton University press, Princeton
Thorne K. S., 1980, Reviews of Modern Physics, 52, 299
Unno W., Osaki Y., Ando H., Saio H., Shibahashi H., 1989, Nonradial oscillations of stars. Tokyo: University of Tokyo Press, 1989, 2nd ed.
Villain L., Bonazzola S., Haensel P., 2005, Phys. Rev. D, 71, 083001
Watts A. L., Strohmayer T. E., 2007, Advances in Space Research, 40, 1446
Yoshida S., Lee U., 2000, ApJS, 129, 353